ACS OMEGA

Open Access

http://pubs.acs.org/journal/acsodf

Article

Investigating the Role of Surface Confinement and Reaction Dynamics in the Production of Polyphenol-Based Nanoparticles

Wei-Ting Chang, Ji-Young Lee, and Leila F. Deravi*

Cite This: *ACS Omega* 2025, 10, 3930−3936

Read Online

ACCESS | Metrics & More | Article Recommendations | Supporting Information

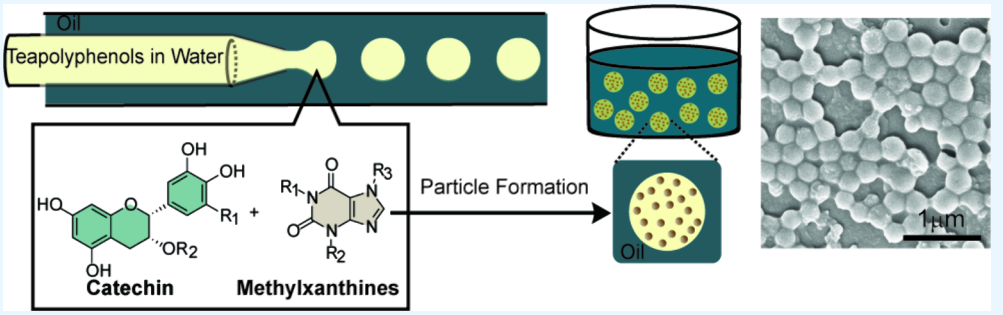

ABSTRACT: The use of polyphenol-based particles as functional materials has demonstrated great promise for applications ranging from targeted therapeutics to environmental remediation due to their biocompatibility, potent reactivity, and modular chemistry. Despite these rich benefits, polyphenols remain difficult to formulate with due to their susceptibility to spontaneous aggregation in aqueous environments. In this study, we explore conditions that leverage this aggregation as a feature to seed the production of monodispersed (polydispersity index of <0.1) nanoparticles with controlled diameters <200 nm. To accomplish this goal, we evaluated the assembly dynamics of a heterogeneous population of green tea extracts in water and investigated the interplay between temperature, time, and surface confinement in both fixed vessels and emulsion droplets on particle size and uniformity. In both cases, homogeneous nanoparticles are created, highlighting a feasible pathway to control and scale the production of polyphenolic nanostructures for future materials applications.

INTRODUCTION

Polyphenols have garnered increasing interest as materials for applications in tissue engineering,[1,2] drug delivery,[3−5] and water remediation[6−9] due in large part to the high reactivity of the core phenolic groups. This reactivity facilitates self-assembly, hydrogen bonding, and extended conjugation, enabling the creation of multifunctional structures that possess key advantages.[9−11] For instance, in drug delivery, polyphenol-based nanoparticles (NPs) enhance vehicle efficiency and safety due to their high antioxidant and anti-inflammatory properties, improving cell uptake and bioavailability.[12−15] The incorporation of polyphenols has also been shown to inhibit quorum sensing, disrupting bacterial binding and biofilm formation through controlled competitive binding events.[16,17] In cell-free applications, polyphenol chemistries applied in filtration systems have been reported to enhance entrapment of organic dyes and/or chelation of inorganic salts in waste streams.[6−9,18] Despite these extraordinary capabilities, there is no universal source of polyphenols, and this variability continues to impact quality control and uniformity of products when investigated in materials applications.[12,14]

Polyphenols can be sourced from various types of biomass, including phenolic acids, nonflavonoids, flavonoids, and polyphenol-rich extracts. Among them, tea leaves are some of the most abundant sources of polyphenols in nature. In fact, the fabrication and use of tea polyphenol nanoparticles (TPNPs) have been explored in numerous studies due their inherent self-assembly and retained functionality, which can be tuned by reaction conditions such as time, starting concentrations, temperature, and volume.[13,19−23] Despite reported successes, TPNPs presented in the literature are typically produced at low (∼1 mg/mL) concentrations and small (∼mL) reaction scales.[13,19−23]

To address these limitations, we explored conditions to control the nucleation and growth of concentrated polyphenols extracted from green tea leaves. We optimized the synthesis and systematically evaluated the effects of reaction surface curvature, time, and temperature on nanoparticle diameter and polydispersity. To introduce a pathway for scalability, we transitioned the batch-processed reaction conditions from our

Received: October 25, 2024
Revised: January 13, 2025
Accepted: January 20, 2025
Published: January 27, 2025

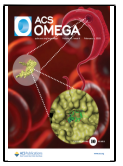

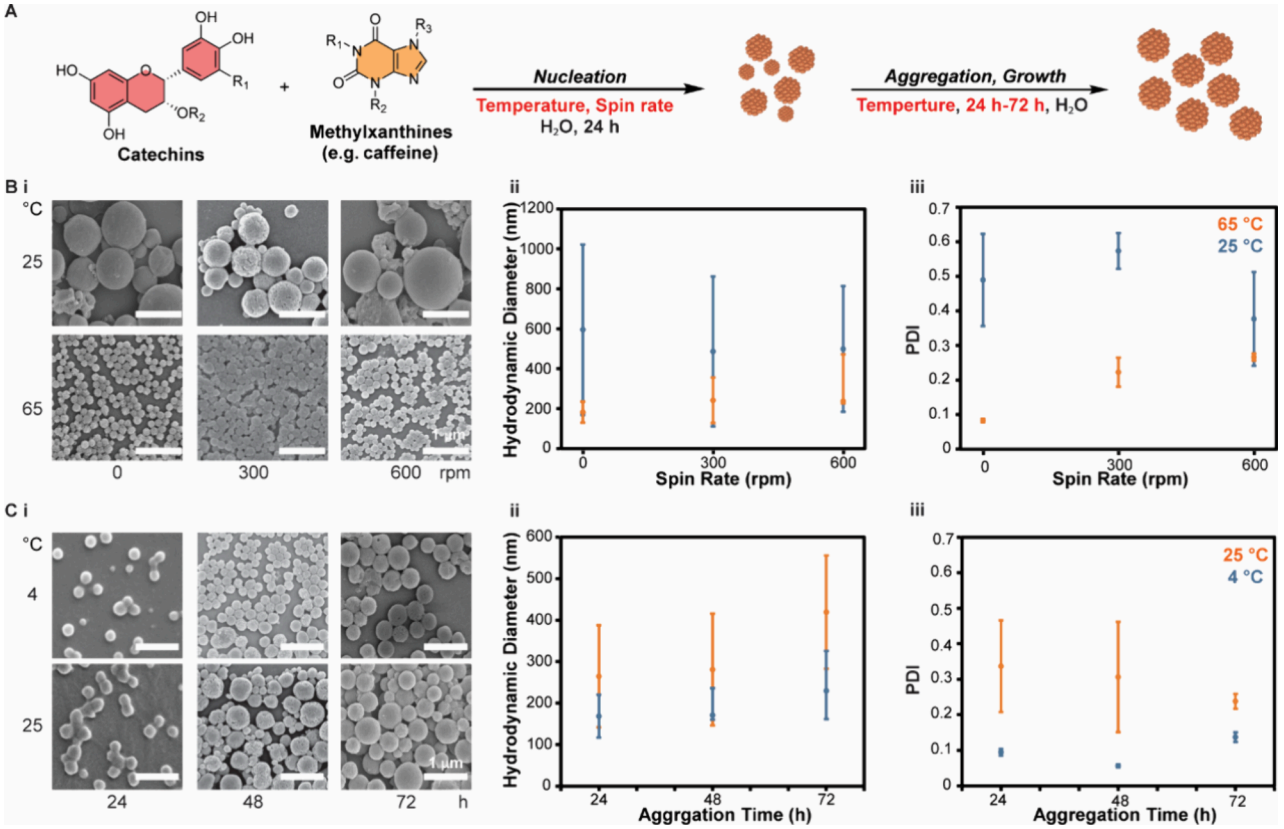

Figure 1. Optimization of TPNP synthesis. (A) Illustration of TPNP formation, highlighting key variables for scaling production, indicated in red. (B) TPNP formation in the nucleation stage. (i) Representative SEM images of TPNPs at the various temperatures (25 °C (top) and 65 °C (bottom)) with the various spin rates (0, 300, and 600 rpm). (ii) Analysis of the hydrodynamic diameter versus the spin rate at 25 and 65 °C. (iii) Analysis of PDI versus the spin rate at 25 and 65 °C. (C) TPNP formation in the aggregation stage. (i) Representative SEM images of TPNPs at the various temperatures (4 °C (top) and 25 °C (bottom)) over time (24, 42, 48, and 72 h). (ii) The hydrodynamic diameter versus reaction time at 4 and 25 °C. (iii) Analysis of PDI versus the reaction time at 4 and 25 °C. All particle sizes and PDIs were measured by dynamic light scattering (DLS) in triplicate and recorded as mean ± standard deviation (S.D.). All scale bars correspond to 1 μm.

fixed vessels to a continuous flow system designed to replicate the surface confinement needed for consistent TPNP production. We validated feasibility using a microfluidic chip, where TPNPs are produced within water-in-oil (W/O) emulsion droplets and subjected to controlled thermocycling to produce homogeneous nanoparticles. This development offers a scalable approach to produce robust TPNPs at concentrations 100 times higher than previous reports with product yields of 1 mg/batch (static conditions) and 155 mg/batch (from emulsion droplet conditions).

RESULTS AND DISCUSSION

Inspired by recent findings that theophylline can act as a cross-linker to strengthen intermolecular interactions needed for TPNP formation,[19] we explored combinations of theophylline with tea polyphenols (TPs) to scale the production of these particles. Li and co-workers established that TPNP formation is initiated in solution at 1 mg/mL in the presence of theophylline in air (80 °C for 30 h); after which point, NP precipitation occurs during a room temperature incubation (48 h), which they claim occurs via oxidative polymerization.[19] We explored conditions to scale this process by carefully adjusting: (1) the concentration and ratio of the TP precursor with theophylline, (2) the reaction temperature, and (3) the stirring rate (Figure 1A). Through our combinatorial approach, we identified parameters that significantly influence the physical characteristics of the TPNPs, including morphology, particle size, and polydispersity at higher starting concentrations.

To start, we varied the ratio of TPs and theophylline in the initial reaction and observed that 32 mg/mL tea extract with 0.6 mg/mL theophylline in water was the maximum achievable concentration for creating particles (Table S1). To achieve TPNPs with a polydispersity index (PDI) below 0.1 (Figure 1B,C, Table S1), we investigated nucleation temperatures (25 and 65 °C) under varying stirring speeds (0, 300, and 600 rpm) on nanoparticle formation. In our experiments, stirring the TP precursors at 600 rpm resulted in TPNPs with a hydrodynamic diameter of 237 ± 122 nm and a PDI of 0.27 ± 0.01 at 65 °C, compared to TPNPs produced at 25 °C, which had a diameter of 499 ± 315 nm and a PDI of 0.38 ± 0.14 (Figure 1B). Interestingly, when no stirring was applied during the nucleation stage at 65 °C, the hydrodynamic diameter of TPNPs was reduced to 182 ± 52 nm with a PDI of 0.08 ± 0.01, indicating that the particles were monodispersed under these conditions (Figure 1B). Based on our analysis, we determined that a static (no stirring) condition at 65 °C produced the smallest diameter particles with the lowest PDI. This condition was used when exploring reaction conditions of the aggregation stage, where we examined how duration and temperature affected nanoparticle diameter and PDI. When the reactors were kept at 4 °C for 48 h, a hydrodynamic size of 171 ± 40 nm and PDI of 0.06 ± 0.00 were achieved in contrast to 169 ± 52 and 230 ± 85 nm particle diameters when incubated

https://doi.org/10.1021/acsomega.4c09744
ACS Omega 2025, 10, 3930−3936

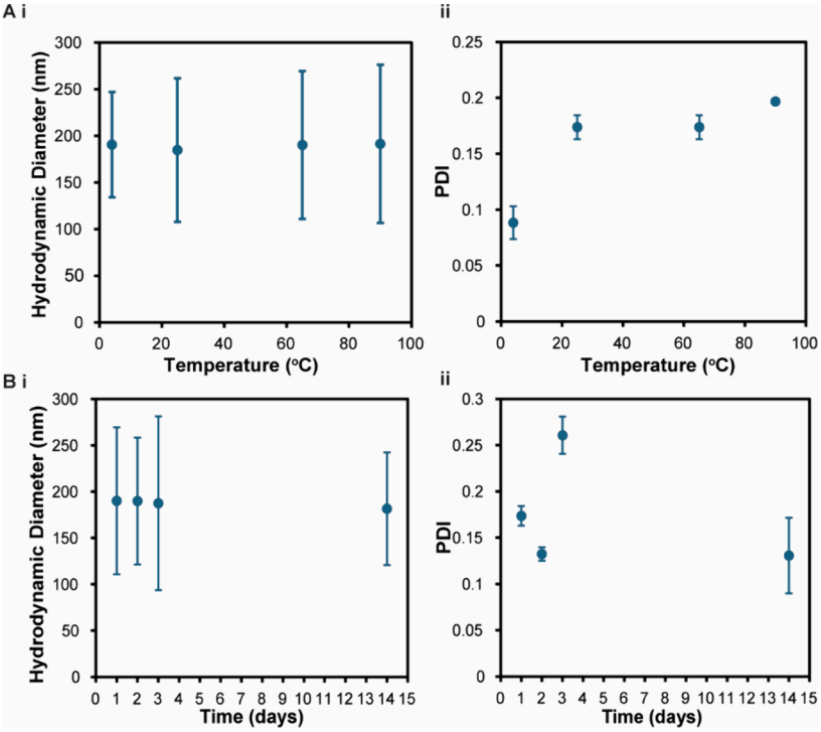

Figure 2. Tracking stability of TPNPs in a 1 wt/v% aqueous solution over time and at varying temperatures. (A) Thermal stability was evaluated by exposing the solution to 4, 25, 65, and 90 °C for 30 min, measuring the effects on (i) hydrodynamic diameters and (ii) PDIs. (B) Storage stability at room temperature was monitored over 1, 2, 3, and 14 days with measurements of (i) hydrodynamic diameters and (ii) PDIs. All particle sizes and PDIs were measured using DLS in triplicate and recorded as mean ± SD.

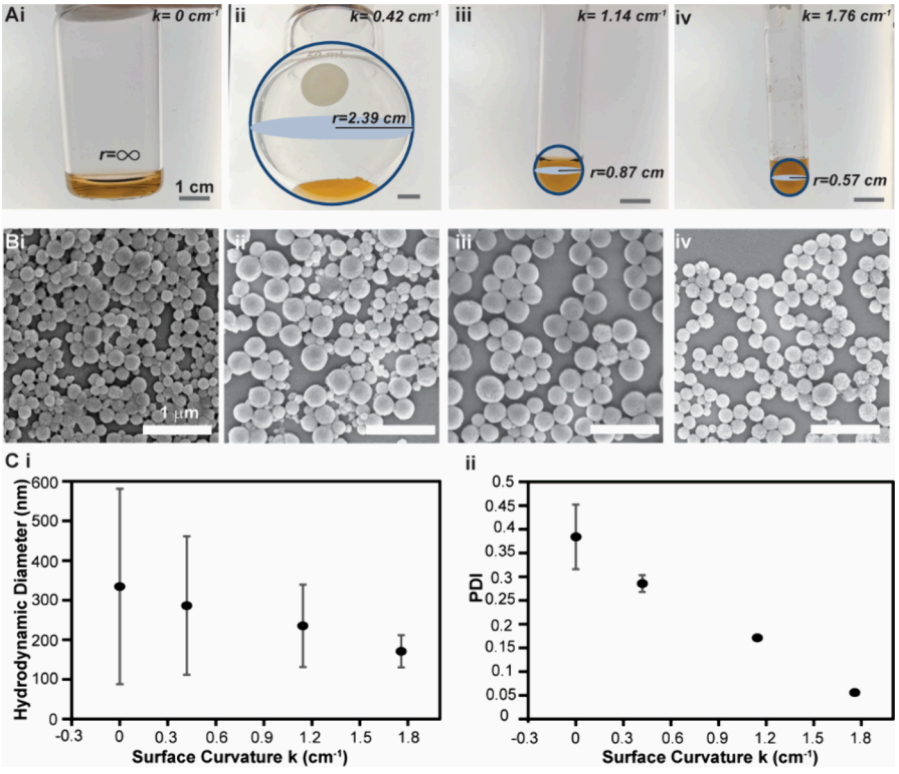

Figure 3. Investigating the influence of surface curvature on TPNP assembly. (A) Images of various vessel sizes tested: (i) a 20 mL flat-bottom vial, (ii) a 50 mL round-bottom flask, (iii) a 15 mL round vial, and (iv) a 10 mL round vial. Scale bar = 1 cm. The surface curvature (k) for each vessel is shown as an inset. (B) Representative SEM images of particles formed in each vessel corresponding to (A). Scale bar = 1 μm. (C) Surface curvature of different vessels impacts (i) hydrodynamic diameters and (ii) PDIs of the particles as measured by DLS. All values were measured in triplicate and recorded as mean ± SD.

https://doi.org/10.1021/acsomega.4c09744
ACS Omega 2025, 10, 3930−3936

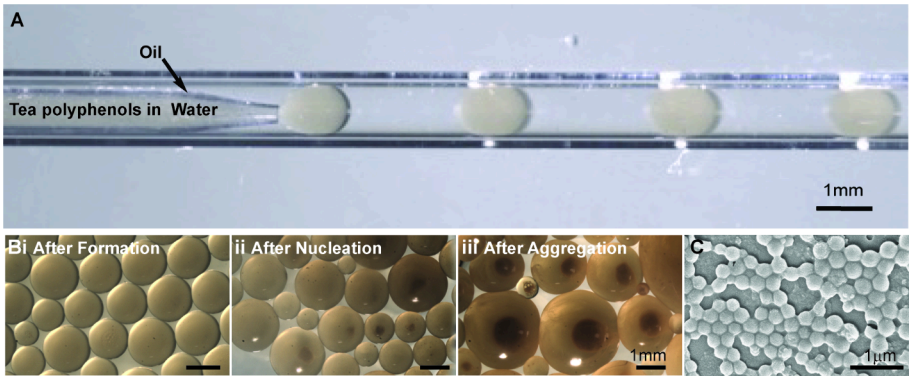

Figure 4. Formation and analysis of TPNPs from W/O emulsion droplets using a microfluidic chip. (A) Bright-field images of the W/O emulsion droplets containing TP precursors were produced using a coflow microfluidic chip. (B) Bright-field images of the droplets at various stages: (i) after formation, (ii) after the nucleation stage (RT, 48 h), and (iii) after the aggregation stage (4 °C, 48 h). (C) Representative SEM image of TPNPs obtained through lysing droplets and subsequent purification. Scale bars in (B) are 1 mm; scale bar in (C) is 1 μm.

for 24 or 72 h at 4 °C (Figure 1C). When reactors were incubated at 25 °C (no stirring) like the Li paper,[19] NPs appeared more uneven with hydrodynamic diameters of 281 ± 135 nm and a PDI of 0.31 ± 0.16 after 48 h (Figure 1C).

To further support the measurements collected on the DLS, we manually measured diameters and calculated the PDI from these values based on particle sizes from our SEM images (n = 100 particles measured across 3 images per condition) in Figure S1. While minor deviations in the average particle sizes were observed in the optimized conditions (182 ± 53 and 197 ± 15 nm for SEM measured vs DLS measured diameters in 65 °C nucleation stage, respectively, and 596 ± 427 and 758 ± 274 nm for SEM measured vs DLS measured diameters in 25 °C nucleation stage, respectively), these differences were not statistically different from one another (p > 0.05). These observations further support that the DLS analysis is appropriate for monitoring reaction optimization in our method. The optimized condition, involving no stirring during the nucleation stage at 65 °C for 1 day and the aggregation stage at 4 °C for 2 days, yields 3% of TPNPs (1 mg) from the initial 32 mg/mL tea extract and 0.6 mg/mL theophylline precursor materials in water.

Stability of TPNPs. Based on our optimization reactions, we identified that nucleation at heated, static conditions (65 °C, no stirring) followed by aggregation under cooled, static conditions (4 °C, no stirring) provided the most uniform particles. We next assessed the storage and thermal stability of the optimized TPNPs in Milli-Q water by analyzing their size and size distribution. For the storage stability assessments, all aqueous suspensions (1 wt/v%) were monitored at room temperature over 2 weeks using DLS. For thermal stability, aqueous suspensions (1 wt/v%) were monitored after 30 min when exposed to cold (4 °C), ambient (25 °C), and heated (65 and 90 °C) conditions. The results revealed hydrodynamic diameters of 191 ± 56, 185 ± 77, 190 ± 79, and 191 ± 85 nm with corresponding PDIs of 0.09 ± 0.03, 0.17 ± 0.02, 0.17 ± 0.01, and 0.19 ± 0.04 after 30 min of incubation at 4, 25, 65, and 90 °C, respectively (Figure 2A). Elevated thermal treatment of TPNPs nearly doubled the PDI while maintaining similar average diameters, suggesting that some aggregation or particle coalescence may be occurring under these conditions. This result is further supported by SEM images, as shown in Figure S3, which indicate that some particles may have aggregated at 65 °C after 30 min. Despite these differences, the particle diameters remained stable during incubation in solution for over 2 weeks at room temperature, with no significant changes observed (original sizes of 190 ± 79 and 182 ± 60 nm after 2 weeks). The slight variations in PDI (original PDI of 0.17 ± 0.01 and 0.13 ± 0.04 after 2 weeks) further confirm the stability of the particles during this period (Figure 2B). Similarly, the zeta potential of TPNPs measured at −40 mV also did not significantly change (Figure S2), indicating that the particle surface chemistry and charge remained consistent under these storage conditions.

Surface Curvature Affects Particle Formation. While we observed promising results from the optimized TPNPs within sealed vials containing only 1 mL of precursor solution (Figure 3), increasing the reaction volume to 3 mL led to noticeable changes in particle morphology (Figure S4A), with particle diameters increasing to 242 ± 80 nm and an increase in PDI to 0.11 (Figure S4B). To evaluate the scalability of the reaction, we tested various sealed vessel types, as we explored how reaction volume and vessel surface curvature (k) influence particle diameter and PDI. In this analysis, surface curvature was defined as $1/r$, where r is the cross-sectional radius of the reaction vessel. We selected four different types of glass vials with varying capacities: a 20 mL flat-bottomed vial (Figure 3Ai), a 50 mL round-bottomed flask (Figure 3Aii), a 15 mL round vial (Figure 3Aiii), and a 10 mL round vial (Figure 3Aiv). At a fixed 1 mL volume, we calculated k as 0, 0.42, 1.14, and 1.76 cm^{-1}, representing the 20 mL flat-bottomed, 50 mL, 15 mL, and 10 mL curved vials, respectively. We observed differences in nanoparticles morphology (Figure 3B) and hydrodynamic diameters (Figure 3Ci) that also correlated with significant changes in PDIs (Figure 3Cii). In all cases, the larger k resulted in a narrower and smaller PDI as well as more uniform diameters. For instance, TPNPs synthesized in a 10 mL sealed round vial with a surface curvature of 1.76 cm^{-1} had a diameter of 171 ± 40 nm and PDI of 0.06 ± 0.01 compared to a 20 mL flat-bottom vial ($k \sim 0$ cm^{-1}), which had a diameter of 335 ± 246 nm and corresponding PDI of 0.38 ± 0.13 (Figure 3C).

Given these observations, we aimed to explore whether maximizing the surface curvature could be achieved without compromising the reaction throughput. To test this, we created water-in-oil (W/O) emulsion droplets containing the TP precursor materials using a coflow microfluidic chip similar to previous work.[24] The device featured an outer channel with a 1 mm inner dimension of a square capillary tube for the oil phase and a tapered circular capillary with a 400 μm diameter

https://doi.org/10.1021/acsomega.4c09744
ACS Omega 2025, 10, 3930−3936

for the inner aqueous TPNP solution (Figure 4A). The flow rates were set at 4 mL/h for the inner aqueous phase and 15 mL/h for the outer oil phase, enabling the formation of stable W/O droplets resulting in the formation of stable W/O droplets. These droplets successfully encapsulated TP precursor materials at concentrations up to 100 mg/mL, which is 100× the concentrations reported in the literature. The generated droplets had an average diameter of 1.6 mm (Figure 4Bi), corresponding to an k value of 12.4 cm^{-1}. Because the W/O droplets ruptured at 65 °C after 1 h, we readjusted the procedure to incubate the nucleation stage at room temperature for 48 h, which was sufficient to generate turbidity in the inner phase (Figure 4Bii). This was followed by an aggregation step at 4 °C for an additional 48 h (Figure 4Biii). Despite these modifications, TPNPs successfully formed (Figure 4C), with a recorded hydrodynamic diameter range of 191 ± 32 nm and a PDI of 0.06 ± 0.00. This modified approach produced 15.5 mg of TPNPs from a total of 100 mg/mL of TP precursor and 1 mL/mL of theophylline, representing a 16% yield, compared to the 3% yield achieved under static vessel conditions. We attributed this increase in yield to the higher exposed surface curvature of the emulsion droplets, further supporting a scalable pathway for enhanced TPNP production.

CONCLUSIONS

In this study, we developed a reproducible method for generating <200 nm TPNPs up to concentrations 100 times higher than previously reported. In our attempts to scale production, we discovered a strong dependence of nanoparticle uniformity on the exposed surface curvature of the reaction vessel, which may have previously limited the scalability of these nanoparticles. While these direct correlations are still under investigation, we were able to leverage this insight in the design of W/O emulsions that maximize exposed surface curvature to scale the production of TPNPs in droplets. This breakthrough introduces a realistic pathway to move beyond benchtop fabrication toward more industrial scales, which is critical for future materials applications. While our work focused on polyphenol extracts from green tea, we believe that this method can be adapted for other phenolic starting materials, expanding the potential application space of these valuable biomaterials.

MATERIALS AND METHODS

Synthesizing TPNPs. TPNPs were synthesized by dissolving a green tea polyphenol (TP) powder (32 mg, tea extract, 4:1, powder from hydroglycolic extraction of *Camellia sinensis*, Spectrum chemical) and theophylline (0.6 w/w %, Sigma-Aldrich) in 1 mL of Milli-Q deionized water inside a 10 mL sealed tube. The mixture was heated to 65 °C for 24 h without stirring. Afterward, the solution was allowed to cool naturally and was stored undisturbed at 4 °C for 2 days. The TPNPs were then isolated by centrifugation at 2350g for 30 min and rinsed three times with deionized water via centrifugation at 21150g for 30 min each time to obtain the brown precipitate. The final product was stored at 4 °C for later use.

CHARACTERIZATION OF TP PARTICLES

Dynamic Light Scattering. The hydrodynamic diameter, polydispersity index (PDI), and zeta potential were measured by using a Malvern Nano ZS 90. All measurements were conducted at 10 mg/mL of sample at 25 °C. All particle sizes and PDIs were tested by DLS in triplicate.

Scanning Electron Microscopy (SEM) Imaging. SEM images of the particles were captured by using a Hitachi S4800 field emission SEM microscope. The particle samples were washed three times with deionized water, diluted, drop-cast onto glass slides, dried, and coated with platinum using a sputter coater (Cressington 108 Auto). The analysis was performed at a voltage of 3 kV and a current of 10 mA.

Surface Curvature Measurements. A total of 0.032 g of TP powder and 0.6 mg of theophylline were dissolved in 1 mL of Milli-Q deionized water in various vessels (10 mL round vial, 15 mL round vial, 50 mL round-bottom flask, and 20 mL flat vial) without stirring. The solution was then heated to 65 °C for 24 h. Size analysis of the TP nanoparticles was conducted on the different surface curvatures, and representative SEM images of the particles were obtained.

To estimate the curvature magnitude, the curvature of a differentiable curve was defined by the osculating circle, which best approximates the curve at a given point. The surface curvature (k) was calculated using the radius (r) of the containers, following the equation: $k = 1/r$. The radius of the containers was measured through simulations of reactor curvature using ImageJ.[25]

Fabrication of Water-in-Oil Emulsions. The coflow microfluidic device was constructed by inserting a tapered circular capillary into a square capillary. Circular capillary tubes with inner and outer diameters of 0.6 and 0.84 mm (VitroCom) were tapered using a micropipet puller (P-1000, Sutter Instrument Inc.), and the final diameter of 400 μm was achieved by sanding with fine-grit sandpaper. The tapered circular capillary tube was treated with n-octadecyltrichlorosilane (Thermo Scientific Chemicals) to enhance the wettability of the oil phase. The aqueous phase, containing 100 mg/mL TP precursor materials, flowed through the tapered circular capillary at a rate of 4 mL/h, while the oil phase, consisting of fluorocarbon oil (HFE 7500, 3M) with 5 w/w % surfactant (Krytox 157FSH, DuPont), flowed through the square capillary at a rate of 15 mL/h. This configuration enabled coaxial flow, optimizing the fluid interface for stable W/O emulsions. The droplets were all formed at room temperature within 20 min. The droplets were then stored in a sealed vial containing 10 mL of fluorocarbon oil. Under these conditions, nucleation at room temperature occurred within 2 days. This was then followed by aggregation at 4 °C for an additional 48 h to form nanoparticles within the emulsions. The TPNPs were then isolated by breaking the emulsion via vortex mixing followed by density-based separation and purification through multiple centrifugations and washing for three cycles.

ASSOCIATED CONTENT

Supporting Information

The Supporting Information is available free of charge at https://pubs.acs.org/doi/10.1021/acsomega.4c09744.

These include the detailed parameters and results of the TPNP formation (Table S1), thermostability (Figures S1−S3), and variables influencing scalability (Figure S4 and Table S2) (PDF)

https://doi.org/10.1021/acsomega.4c09744
ACS Omega 2025, 10, 3930−3936

AUTHOR INFORMATION

Corresponding Author

Leila F. Deravi − *Department of Chemistry and Chemical Biology, Northeastern University, Boston, Massachusetts 02115, United States;* orcid.org/0000-0003-3226-2470; Email: l.deravi@northeastern.edu

Authors

Wei-Ting Chang − *Department of Chemistry and Chemical Biology, Northeastern University, Boston, Massachusetts 02115, United States*

Ji-Young Lee − *Department of Chemistry and Chemical Biology, Northeastern University, Boston, Massachusetts 02115, United States*

Complete contact information is available at: https://pubs.acs.org/10.1021/acsomega.4c09744

Author Contributions

The manuscript was written through contributions of all authors. All authors have given approval to the final version of the manuscript.

Notes

The authors declare no competing financial interest.

ACKNOWLEDGMENTS

The authors would like to thank Dr. Shirin Kaboli and the Boston Electron Microscopy Center Facility for their help in the SEM analysis. In addition, the authors would also like to acknowledge partial support from NSF DMR-1945207, the Department of Chemistry and Chemical Biology at Northeastern University, and the Army Research Office as accomplished under Cooperative Agreement Number W911NF-22-2-0119. The views and conclusions contained in this document are those of the authors and should not be interpreted as representing the official policies, either expressed or implied, of the Army Research Office or the U.S. Government. The U.S. Government is authorized to reproduce and distribute reprints for Government purposes notwithstanding any copyright notation herein.

REFERENCES

(1) Zhang, X.; Li, Z.; Yang, P.; Duan, G.; Liu, X.; Gu, Z.; Li, Y. Polyphenol scaffolds in tissue engineering. *Materials Horizons* **2021**, *8*, 145−167.

(2) Li, Z.; Chen, Z.; Chen, H.; Chen, K.; Tao, W.; Ouyang, X.-k.; Mei, L.; Zeng, X. Polyphenol-based hydrogels: Pyramid evolution from crosslinked structures to biomedical applications and the reverse design. *Bioactive Materials* **2022**, *17*, 49−70.

(3) Fu, X.; Zhang, Y.; Zhang, G.; Li, X.; Ni, S.; Cui, J. Targeted delivery of Fenton reaction packages and drugs for cancer theranostics. *Applied Materials Today* **2022**, *26*, No. 101353.

(4) Zhou, J.; Lin, Z.; Ju, Y.; Rahim, M. A.; Richardson, J. J.; Caruso, F. Polyphenol-Mediated Assembly for Particle Engineering. *Acc. Chem. Res.* **2020**, *53*, 1269−1278.

(5) Shin, M.; Park, E.; Lee, H. Plant-Inspired Pyrogallol-Containing Functional Materials. *Adv. Funct. Mater.* **2019**, *29*, No. 1903022.

(6) Su, X.; Xie, W.; Wang, P.; Tian, Z.; Wang, H.; Yuan, Z.; Liu, X.; Huang, J. Strong underwater adhesion of injectable hydrogels triggered by diffusion of small molecules. *Materials Horizons* **2021**, *8*, 2199−2207.

(7) Liu, H.; Geng, H.; Zhang, X.; Wang, X.; Hao, J.; Cui, J. Hot Melt Super Glue: Multi-Recyclable Polyphenol-Based Supramolecular Adhesives. *Macromol. Rapid Commun.* **2022**, *43*, No. 2100830.

(8) Cheng, B.; Yu, J.; Arisawa, T.; Hayashi, K.; Richardson, J. J.; Shibuta, Y.; Ejima, H. Ultrastrong underwater adhesion on diverse substrates using non-canonical phenolic groups. *Nat. Commun.* **2022**, *13*, 1892.

(9) Xu, Y.; Hu, J.; Zhang, X.; Yuan, D.; Duan, G.; Li, Y. Robust and multifunctional natural polyphenolic composites for water remediation. *Materials Horizons* **2022**, *9*, 2496−2517.

(10) Geng, H.; Zhong, Q.-Z.; Li, J.; Lin, Z.; Cui, J.; Caruso, F.; Hao, J. Metal Ion-Directed Functional Metal−Phenolic Materials. *Chem. Rev.* **2022**, *122*, 11432−11473.

(11) Koch, W.; Zagórska, J.; Marzec, Z.; Kukula-Koch, W. Applications of Tea (Camellia sinensis) and Its Active Constituents in Cosmetics. *Molecules* **2019**, *24*, 4277.

(12) Yang, P.; Zhang, J.; Xiang, S.; Jin, Z.; Zhu, F.; Wang, T.; Duan, G.; Liu, X.; Gu, Z.; Li, Y. Green Nanoparticle Scavengers against Oxidative Stress. *ACS Appl. Mater. Interfaces* **2021**, *13*, 39126−39134.

(13) Chen, Z.; Wang, C.; Chen, J.; Li, X. Biocompatible, Functional Spheres Based on Oxidative Coupling Assembly of Green Tea Polyphenols. *J. Am. Chem. Soc.* **2013**, *135*, 4179−4182.

(14) Wahnou, H.; Liagre, B.; Sol, V.; El Attar, H.; Attar, R.; Oudghiri, M.; Duval, R. E.; Limami, Y. Polyphenol-Based Nanoparticles: A Promising Frontier for Enhanced Colorectal Cancer Treatment. *Cancers* **2023**, *15*, 3826.

(15) De Matteis, V.; Cascione, M.; Rizzello, L.; Manno, D. E.; Di Guglielmo, C.; Rinaldi, R. Synergistic Effect Induced by Gold Nanoparticles with Polyphenols Shell during Thermal Therapy: Macrophage Inflammatory Response and Cancer Cell Death Assessment. *Cancers* **2021**, *13*, 3610.

(16) Wang, T.; Zhang, J.; Zhang, H.; Bai, W.; Dong, J.; Yang, Z.; Yang, P.; Gu, Z.; Li, Y.; Chen, X.; Xu, Y. Antioxidative myricetin-enriched nanoparticles towards acute liver injury. *J. Mater. Chem. B* **2022**, *10*, 7875−7883.

(17) Li, H.; Zhang, J.; Yang, L.; Cao, H.; Yang, Z.; Yang, P.; Zhang, W.; Li, Y.; Chen, X.; Gu, Z. Synergistic Antimicrobial and Antibiofilm Nanoparticles Assembled from Naturally Occurring Building Blocks. *Adv. Funct. Mater.* **2023**, *33*, No. 2212193.

(18) Wang, T.; Zhao, J.; Yang, Z.; Xiong, L.; Li, L.; Gu, Z.; Li, Y. Polyphenolic sunscreens for photoprotection. *Green Chem.* **2022**, *24*, 3605−3622.

(19) Xiang, S.; Yang, P.; Guo, H.; Zhang, S.; Zhang, X.; Zhu, F.; Li, Y. Green Tea Makes Polyphenol Nanoparticles with Radical-Scavenging Activities. *Macromol. Rapid Commun.* **2017**, *38*, No. 1700446.

(20) Ninsiima, H. I.; Eze, E. D.; Ssekatawa, K.; Nalugo, H.; Asekenye, C.; Onanyang, D.; Munanura, E. I.; Ariong, M.; Matama, K.; Zirintunda, G.; Mbiydzenyuy, N. E.; Ssempijja, F.; Afodun, A. M.; Mujinya, R.; Usman, I. M.; Asiimwe, O. H.; Tibyangye, J.; Kasozi, K. I. Green tea silver nanoparticles improve physiological motor and cognitive function in BALB/c mice during inflammation. *Heliyon* **2023**, *9*, No. e13922.

(21) Markova, Z.; Novak, P.; Kaslik, J.; Plachtova, P.; Brazdova, M.; Jancula, D.; Siskova, K. M.; Machala, L.; Marsalek, B.; Zboril, R.; Varma, R. Iron(II,III)−Polyphenol Complex Nanoparticles Derived from Green Tea with Remarkable Ecotoxicological Impact. *ACS Sustainable Chem. Eng.* **2014**, *2*, 1674−1680.

(22) Chen, G.; Yi, Z.; Chen, X.; Ma, X.; Su, W.; Li, X. Polyphenol Nanoparticles from Commonly Consumed Tea for Scavenging Free Radicals, Stabilizing Pickering Emulsions, and Inhibiting Cancer Cells. *ACS Applied Nano Materials* **2021**, *4*, 652−665.

(23) Chung, J. E.; Tan, S.; Gao, S. J.; Yongvongsoontorn, N.; Kim, S. H.; Lee, J. H.; Choi, H. S.; Yano, H.; Zhuo, L.; Kurisawa, M.; Ying, J. Y. Self-assembled micellar nanocomplexes comprising green tea catechin derivatives and protein drugs for cancer therapy. *Nat. Nanotechnol.* **2014**, *9*, 907−912.

(24) Kim, J.-H.; Lee, J.-Y.; Kim, J.; Gong, Z.; Wilson, D. J.; Deravi, L. F.; Lee, D. Adaptive coloration enabled by the reversible osmotic annealing of chromatophore-like microcapsules. *Journal of Materials Chemistry C* **2024**, *12*, 2148−2155.

(25) Blasjo, V. *Transcendental Curves in the Leibnizian Calculus. Studies in the History of Mathematical Inquiry*; Academic Press: 2017.

https://doi.org/10.1021/acsomega.4c09744
ACS Omega 2025, 10, 3930−3936